Order-disorder type critical behavior at the magnetoelectric phase transition in multiferroic $DyMnO_3$

M. Schiebl,[1] A. Shuvaev,[1] Anna Pimenov,[1] G. E. Johnstone,[1] V. Dziom,[1] A. A. Mukhin,[2] V. Yu. Ivanov,[2] and A. Pimenov[1]
[1]*Institute of Solid State Physics, Vienna University of Technology, A-1040 Vienna, Austria*
[2]*Prokhorov General Physics Institute, Russian Academy of Sciences, 119991 Moscow, Russia*
(Received 10 March 2015; revised manuscript received 8 May 2015; published 29 June 2015)

We present the results of detailed dielectric investigations of the relaxation dynamics in $DyMnO_3$ multiferroic manganite. A strong low-frequency relaxation process near the paraelectric-ferroelectric phase transition is observed. We provide experimental evidence to show that this relaxation mode corresponds to a chirality switching of the spin cycloid in $DyMnO_3$. We demonstrate that the relaxation dynamics in $DyMnO_3$ is typical for an order-disorder phase transition and may be understood within a simple model with a double-well potential. These results suggest the interpretation of the paraelectric sinusoidal phase in manganites as a dynamical equilibrium of magnetic cycloids with opposite chiralities.

DOI: 10.1103/PhysRevB.91.224205 PACS number(s): 77.55.Nv

I. INTRODUCTION

Multiferroic materials with a coupling of electric and magnetic degrees of freedom have attracted considerable interest since the discovery of a large magnetoelectric effect (ME) in several compounds [1–4]. They are currently the subject of intensive study due to their fascinating physical properties and the potential for applications as multifunctional devices [5,6]. The rare-earth $RMnO_3$ manganites (R = Gd, Tb, Dy, or Eu/Y) with orthorhombically distorted perovskite structure have emerged as a new class of multiferroics with strongly coupled antiferromagnetic and ferroelectric properties [7,8]. Several rare-earth manganites order antiferromagnetically below $T_N \sim 40$ K into a collinear paraelectric phase [9] with sinusoidal modulations of spins. This phase is followed by a cycloidal spin order with nonzero electric polarization below $T_C \sim 20$ K.

It should be noted that the Mn^{3+} atom is supposed [10] to have a Heisenberg spin with a fixed length of $S = 2$. The purely sinusoidally modulated spin phase contradicts this property. Model calculations [10] have obtained the sinusoidal order only as a time-space average of the simulated cluster. Thus, there is a possibility that a short-range dynamic order exists in the intermediate temperature range $T_C < T < T_N$, which is responsible for the "hidden" spin. As the magnetic order at low temperatures is a spin cycloid, it is natural to assume that the dynamic short-range order is also a spin cycloid. This would imply that there are fluctuating ferroelectric regions in the sinusoidal phase and that the ferroelectric transition is actually of the order-disorder type. Such a transition has also been suggested in Ref. [11], where c-axis relaxation typical for the order-disorder type transitions has been investigated. The fact that the wave vector q_{Mn} of the spin wave does not change at the transition temperature T_C [12] is also indirect evidence that the ferroelectric transition is not of the displacive type.

The data by terahertz spectroscopy [13,14] evidence the nonzero dielectric contribution of an electromagnon in the sinusoidal phase. According to the commonly accepted mechanism of the electromagnon [15,16], the majority of the spectral weight of this mode originates from an exchange striction mechanism and can only exist in magnetic phases with a noncollinear spin arrangement. These facts again favor the hypothesis of dynamical cycloidal spin order in the sinusoidal phase.

Recent theoretical analysis of the terahertz dynamics in the sinusoidal phase suggested an explanation based on anomalous magnetoelectric coupling. Investigations of the collinear sinusoidal phase in the diluted compounds $TbMn_{1-x}Al_xO_3$ [17] and the observation of the memory effect in the low-temperature sinusoidal phase in the multiferroic $MnWO_4$ [18] have suggested the presence of nanosized ferroelectric domains and support a relaxor order-disorder type transition.

In this work, we present an analysis of the critical behavior of the low-frequency relaxation in $DyMnO_3$. The observed critical behavior confirms that the sinusoidal to cycloidal phase transition is of order-disorder type. Our model suggests the presence of short-range cycloidal order in the collinear spin phase.

A. $DyMnO_3$

In zero magnetic field, $DyMnO_3$ undergoes an antiferromagnetic (AFM) transition with a temperature-dependent modulation vector ($0\ q_{\mathrm{Mn}}\ 1$) around $T_N = 39$ K. With further cooling, the q_{Mn} value is locked at the transition temperature, $T_C \approx 19$ K, and ferroelectric (FE) polarization appears simultaneously along the c axis. It is well established that the ferroelectric polarization in $DyMnO_3$ is induced by a cycloidal magnetic order [9,10,12] through the inverse Dzyaloshinskii-Moriya (DM) interaction [4,19–21], and it can be written as

$$P = \sum_{i,j} K e_{i,j} \times (S_i \times S_j), \tag{1}$$

where $e_{i,j}$ denotes the unit vector connecting the spins S_i and S_j, and K is a constant representing the exchange interaction and the spin-orbit interaction. Accordingly, the electric polarization, P, is intimately linked to the chirality of the magnetic cycloid (clockwise and counterclockwise cycloidal magnetic ordering, respectively), that is, changing the direction of $+P \rightarrow -P$ implies changing the rotation (chirality) of the magnetic cycloid. This was demonstrated [22] by the asymmetry in the scattering of left-hand and right-hand circularly polarized x rays by nonresonant magnetic x-ray diffraction for the similar compound $TbMnO_3$.

The unique cycloidal magnetic ordering below T_C in $RMnO_3$ perovskites is assigned to the Mn $3d$ spins [7,9,23–27], but ordering of the Dy $4f$ moments in $DyMnO_3$ is also of interest [9,28,29]. Although it is the magnetic structure of the Mn subsystem that determines the emergence of ferroelectricity in rare-earth manganites [29], the mutual coupling of the Mn $3d$ and Dy $4f$ moments and, consequently, the ordering of the $4f$ moments in Dy causes a particularly large polarization observed in this material [7,30,31]. In addition, the basal plane of the spin cycloid flops from the bc plane to the ab plane and rotates the polarization by applying a magnetic field along the b axis.

With regard to the temperature range $T_C < T < T_N$, there have been a number of studies of the magnetic structure of $DyMnO_3$ and the related material $TbMnO_3$ using techniques such as neutron diffraction [9,32] and magnetic x-ray scattering [24,33]. These studies have all shown that there is a long-range sinusoidal magnetic ordering of the Mn^{3+} ions in this temperature range, with the moments aligned parallel to the crystallographic b axis, although Mannix *et al.* [24] and Wilkins *et al.* [33] both show a small component of the moment is aligned with the c axis.

II. EXPERIMENT

$DyMnO_3$ single crystals were grown in Ar flow by a floating-zone method with radiation heating [34,35]. Terahertz properties of the samples from the same batch have been presented previously [36,37]. The complex dielectric constant was measured for an electric field along the crystallographic a axis in the frequency range 0.1 Hz–1 MHz using a frequency response analyzer in magnetic fields 0–14 T and with the $B \| b$ axis. We investigated the temperatures near the critical temperature of the paraelectric-ferroelectric phase transition (red circles in Fig. 2) with an increment of $\Delta T = 0.1$ K by using a physical property measurement system (PPMS). Silver paint contacts were applied to the sample forming a capacitor.

III. PSEUDOSPIN MODEL

The theory of dynamic critical phenomena for a multivariable system can be formulated as a generalization of the single-particle Langevin equation. The equation of motion for the time-dependent local configuration of the order parameter field is most conveniently given by the time-dependent Ginzburg-Landau equation [38–40],

$$\frac{\partial P(\mathbf{r},t)}{\partial t} = -\Gamma \frac{\delta F}{\delta P(\mathbf{r},t)} + \zeta(\mathbf{r},t). \tag{2}$$

Here, the order parameter is given by the static electric polarization P, Γ is a dissipation parameter, and $\zeta(\mathbf{r},t)$ is a random noise simulating the effect of thermal excitation of the order parameter. To guarantee that the system reaches the canonical equilibrium probability distribution at long times, $\zeta(\mathbf{r},t)$ is a random Gaussian variable satisfying $\langle \zeta(\mathbf{r},t) \rangle = 0$ and $\langle \zeta(\mathbf{\acute{r}},t)\zeta(\mathbf{r},\acute{t}) \rangle = 2Dk_BT\delta(\mathbf{r}-\mathbf{\acute{r}})\delta(t-\acute{t})$ [41], where D is the diffusion coefficient. The crucial point is to find an expression for the free energy in Eq. (2). In the framework of the Landau theory for a second-order phase transition, Smolenskii [42] introduced a biquadratic term ($F \propto \gamma P^2 M^2$, magnetodielectric effect) into the free energy that accounts for the coupling between magnetization and electric polarization. Biquadratic terms are invariant to all symmetry operations, and thus they are allowed in any material with coupled spin and charge degrees of freedom. Since the dielectric susceptibility is determined by taking the second derivative of the free energy with respect to the polarization, the dielectric constant will be proportional to the square of the order parameter, $\varepsilon \propto M^2$ [43]. Describing magnetodielectric effects in antiferromagnetic materials, the expression $F \propto \gamma P^2 M^2$ is not sufficient since the magnetization, M, remains zero in the ordered phase. In such a case, M is replaced by the antiferromagnetic vector, $L = M_1 - M_2$. Here M_1 and M_2 are the magnetizations of two antiferromagnetic subsystems.

Within a more general model, Lawes [44,45] *et al.* proposed the coupling of the polarization to the q-dependent magnetic correlation function $\langle M_q M_{-q} \rangle$. This coupling leads to a magnetodielectric term in the free energy, $F \propto \sum_q g(q) P^2 \langle M_q M_{-q} \rangle$, where $g(q)$ is a q-dependent coupling constant. The q dependence of the free energy via a spin-spin correlation function enables us to apply it to very general forms of magnetic order, including ferromagnetic (FM) and antiferromagnetic (AFM) transitions. To obtain a microscopic theory for $g(q)$ in systems with a strong spin-lattice interaction, the coupling between the polarization and the spin correlations arises from the coupling of magnetic fluctuations to the optical phonons. That is, the spin correlations perturb the optical phonon frequencies, which in turn shift the dielectric constant through the spectral weight transfer and the Lyddane-Sachs-Teller relation. The model determines the coupling $g(q)$ by expanding the exchange integral of neighboring spins in terms of the normal coordinates for the phonons. Physically, this procedure corresponds to a coupling between the magnetic correlation function and atomic displacements.

In multiferroic rare-earth manganites, $RMnO_3$, the electric polarization is directly linked to the chirality of the magnetic cycloid [4,20]. Based on this fact, we propose that the polarization in the ferroelectric phase in $DyMnO_3$ is proportional to the difference of opposite chiralities of Mn^{3+} magnetic cycloids. Here we assume an order-disorder type phase transition between paraelectric and ferroelectric states. Similar analysis in a triangular lattice antiferromagnet $RbFe(MoO_4)$ demonstrated a proportionality between polarization in the multiferroic phase and the chirality difference of the magnetic structure [46].

In the present model, the following assumptions for the phase transition in $DyMnO_3$ are imposed: (i) A disorder between clockwise and counterclockwise ab-cycloidal order of the Mn^{3+} magnetic moments is assumed, (ii) the electric dipole moments are associated with the displacement of the O^{2-} ions due to inverse DM interaction [4,20], (iii) the direction of the electric dipoles depends on the chirality of the magnetic order, (iv) two possible directions of the electric dipoles are energetically separated by an energy barrier, and (v) similar to Lawes *et al.* [44,45], we propose a coupling of the magnetic correlation function and the correlation of O^{2-} atomic displacements. Thus we assume that we can describe the ordering of the magnetic sublattice by the ordering process of the O^{2-} ions.

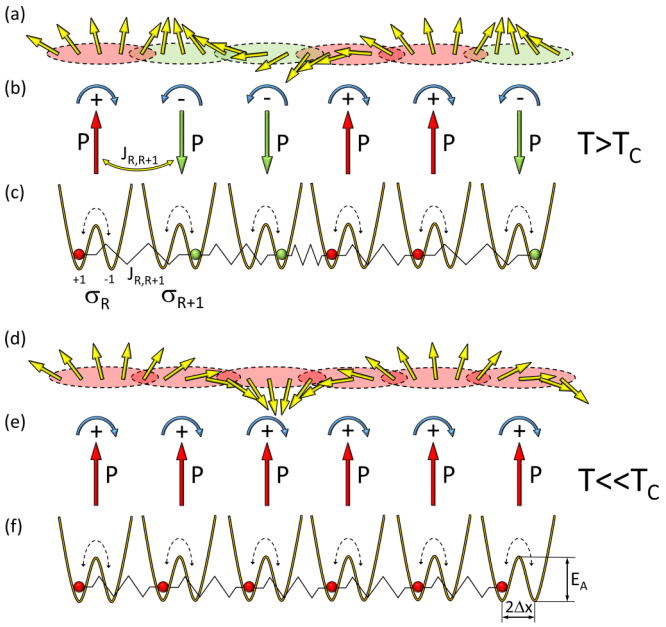

FIG. 1. (Color online) Pseudospin model. (a) Short-range cycloidal order of the Mn^{3+} magnetic moments for $T > T_C$. (b) According to Eq. (1), electric dipoles associated with the O^{2-} ions are generated by the canting of neighboring spins leading to a mesoscopic electric polarization (red and green zones), however the macroscopic electric polarization is zero for $T > T_C$. Each electric dipole interacts with neighboring electric dipoles. (c) Ising-type pseudospins in a local double-well potential separating energetically the clockwise *ab*-cycloidal and the counterclockwise *ab*-cycloidal order of the Mn^{3+} magnetic moments. Each pseudospin is in a local double-well potential and interacts with neighboring pseudospins by harmonic forces, represented as springs. Each pseudospin generates an electric dipole moment of $\mu_R = \sigma_R q \Delta x$. Although the microscopic mechanism of the magnetoelectric coupling is more complex, within the present simple model it is represented as an interaction between neighboring pseudospins via harmonic forces. (d) Long-range cycloidal order of the Mn^{3+} magnetic moments for $T \ll T_C$ and leading to (e) nonzero macroscopic polarization. (f) At low temperatures, most of the pseudospins occupy the same side of the double-well potential.

A useful tool for studying phase transitions is provided by the unidimensional ϕ^4 single-ion model [47–51]. This model contains an array of atoms linked by harmonic forces, with one atom in each unit cell (Fig. 1). Each atom is located in its local double-well potential, which represents the rest of the crystal.

Assuming an order-disorder limit ($E_A/k_BT_C \gg 1$ [52,53]), the system can be described by the pseudospin formalism, and thus the model Hamiltonian is essentially governed by an Ising-type interaction in combination with an interaction of dipoles with a homogeneous electric field [52–54],

$$H \propto -\sum_{R,\acute{R}} \Delta x^2 J_{R,\acute{R}} \sigma_R \sigma_{\acute{R}} - \sum_R E(t) q \Delta x \sigma_R, \qquad (3)$$

where Δx is the displacement of the O^{2-} ion, $J_{R,\acute{R}}$ is the coupling constant between O^{2-} ions at position R and $\acute{R}$, $E(t)$ is a time-dependent homogeneous electric field, q is the charge of the oxygen ion, and σ_R is the pseudospin at position R with $\sigma_R = x_R/\Delta x$, which can take the values $+1$ and -1.

Introducing a statistical mean value of the spin variable, $s = (N_+ - N_-)/(N_+ + N_-)$, with N_+ and N_- being the occupation numbers of O^{2-} ions in the $+1$ and -1 state, respectively, and neglecting fluctuations of correlations, the free energy of the system with polarization $P = nq\Delta x s$ is given by [54]

$$F = -k_BT \ln Z = \int \left\{ \frac{J_0}{nq^2\Delta x} P^2 - nk_BT \times \ln\left[2\cosh\left(\frac{\frac{2\Delta x J_0}{nq} P + E(t) q \Delta x}{k_BT} \right) \right] \right\} dV, \qquad (4)$$

where n is the dipole density and $J_0 = \sum_{\acute{R}} J_{R,\acute{R}}$ represents the coupling constant characterizing the interaction of an O^{2-} ion at position R with another O^{2-} ion at position $\acute{R}$ located within an interaction radius. Since the first term in Eq. (3) is bilinear in the displacements of O^{2-} ions, it corresponds to an electric dipole-dipole interaction.

Expanding F with respect to P and E and taking the functional derivative of F with respect to P leads to an equation of motion of the homogeneous order parameter:

$$\frac{\partial P(t)}{\partial t} = -\Gamma \frac{\delta F}{\delta P} = -\Gamma \left[2\left(\frac{J_0}{nq^2} - \frac{2(\Delta x)^2 J_0^2}{nq^2 k_BT} \right) P + \frac{32(\Delta x)^4 J_0^4}{6n^3 q^4 k_B^3 T^3} P^3 - \frac{2(\Delta x)^2 J_0}{k_BT} E(t) \right]. \qquad (5)$$

Here $\Gamma = nq^2 J_0^{-1} \nu_0 \exp(-E_A/k_BT)$ is the damping parameter.

According to Landau theory [55], the phase transitions takes place when the term in Eq. (5) linear in P vanishes. This determines the phase-transition temperature as $T_C = 2J_0(\Delta x)^2/k_B$. Substituting $E(t) = \delta E \exp(-i\omega t)$ and $P(t) = P_S + \delta P \exp(-i\omega t)$ [56], where P_S is the static electric polarization, and comparing the relaxation rate in a single double-well potential [54,57,58], we get an expression for the relaxation strength $\Delta\varepsilon_r = \delta P/(\varepsilon_0 \delta E)$ and the relaxation time τ in close agreement with Lines and Glass [56] and Blinc and Žekš [59] as

$$\Delta\varepsilon_r^{-1} = \begin{cases} \frac{\varepsilon_0 k_B}{nq^2(\Delta x)^2}(T - T_C), & T > T_C, \\ 2\frac{\varepsilon_0 k_B}{nq^2(\Delta x)^2}(T_C - T), & T < T_C, \end{cases} \qquad (6)$$

$$(2\pi\tau)^{-1} = \begin{cases} \left[\frac{\nu_0}{\pi} \left(\frac{T - T_C}{T} \right) \exp\left(-\frac{E_A}{k_BT} \right) \right], & T > T_C, \\ 2\left[\frac{\nu_0}{\pi} \left(\frac{T_C - T}{T} \right) \exp\left(-\frac{E_A}{k_BT} \right) \right], & T < T_C. \end{cases} \qquad (7)$$

Here ν_0 is the attempt frequency and E_A is the energy barrier separating two local minima (Fig. 1).

Equations (6) and (7) correspond to an order parameter that is homogeneous throughout the entire volume of the crystal. For a spatially dependent order parameter, $P(\mathbf{r})$, and assuming the Gaussian approximation, the relaxation time in Fourier space becomes [38,39]

$$\tau(q)^{-1} = (2a + bq^2)\Gamma, \qquad (8)$$

where $a = A(T - T_C)$, b is a constant, and q is the wave vector. As a consequence, we see that each Fourier component

of the order parameter behaves like an independent particle connected to a spring [39], and the fluctuations in each mode decay with a different relaxation time. Only in the long-wavelength limit, $q = 0$, is the relaxation time in Eq. (8) equal to that in Eq. (7).

In the opposite (displacive) limit of the model, $E_A/k_BT_C \ll 1$, the well-known expressions of Ginsburg-Landau mean-field theory are obtained for $q \to 0$:

$$\Delta\varepsilon_r^{-1} = \begin{cases} \frac{2\varepsilon_0 A}{C}(T - T_C), & T > T_C \\ \frac{4\varepsilon_0 A}{C}(T_C - T), & T < T_C. \end{cases} \tag{9}$$

$$(2\pi\tau)^{-1} = \begin{cases} \frac{\Gamma_d A}{\pi}(T - T_C), & T > T_C \\ \frac{2\Gamma_d A}{\pi}(T_C - T), & T < T_C. \end{cases} \tag{10}$$

Here $A = 3\theta k_B/(8\pi J_0)$, $T_C = \eta/A$, and Γ_d and C are constants of the displacive limit; θ and η are microscopic parameters characterizing the nature of the potential in the ϕ^4 single-ion model [47–51]. *Nota bene*, in canonical ferroelectrics, the ferroelectric phase transition of the displacive type is accompanied by softening of a characteristic phonon. In the long-wavelength limit, an overdamped softening mode is characterized according to Eqs. (9) and (10) [59,60]. Recently, a critical slowing down at the ferroelectric phase transition has been observed in a chiral multiferroic $MnWO_4$ [61]. This behavior has been attributed to an overdamped softening of an electromagnon mode [36,62] obeying the temperature characteristic given in Eqs. (9) and (10) with a critical exponent larger than 1.

IV. RESULTS AND DISCUSSION

As demonstrated in Fig. 2(a), the dielectric permittivity closely follows the known phase diagram of $DyMnO_3$ for the $B\|b$ axis [7]. The changes in the dielectric permittivity are especially strong at the transition to the ferroelectric state with $P\|a$ [Fig. 2(b)]. In addition, a well-pronounced absorption is observed in the close vicinity of T_C [Fig. 2(c)]. Detailed analysis of the low-frequency dielectric relaxation is presented for magnetic fields of 4, 10, and 12 T corresponding to the transition from the sinusoidal paraelectric to the $P\|a$-axis ferroelectric phase.

Figure 3 shows typical dielectric spectra of $DyMnO_3$ close to the ferroelectric transition temperature $T_C \approx 18$ K. The spectra below the megahertz range are dominated by two relaxation processes. Only a wing of the high-frequency relaxation is seen in our spectra because the characteristic frequency of this mode is far above 1 MHz. According to previous dielectric studies, the high-frequency mode can be attributed to the relaxation of the domain walls [63,64] in $DyMnO_3$.

In the following, we concentrate the analysis on an absorption peak observed for frequencies below 1 kHz. As seen already in the spectra in Figs. 3, 2(b), and 2(c), this peak grows in magnitude with decreasing temperature, reaches a maximum value at T_C, and decreases again after passing the critical temperature. The observed dielectric relaxation is slightly asymmetrical with broadening toward low frequencies.

To obtain quantitative information of the origin of the low-frequency mode, the spectra were fitted to the

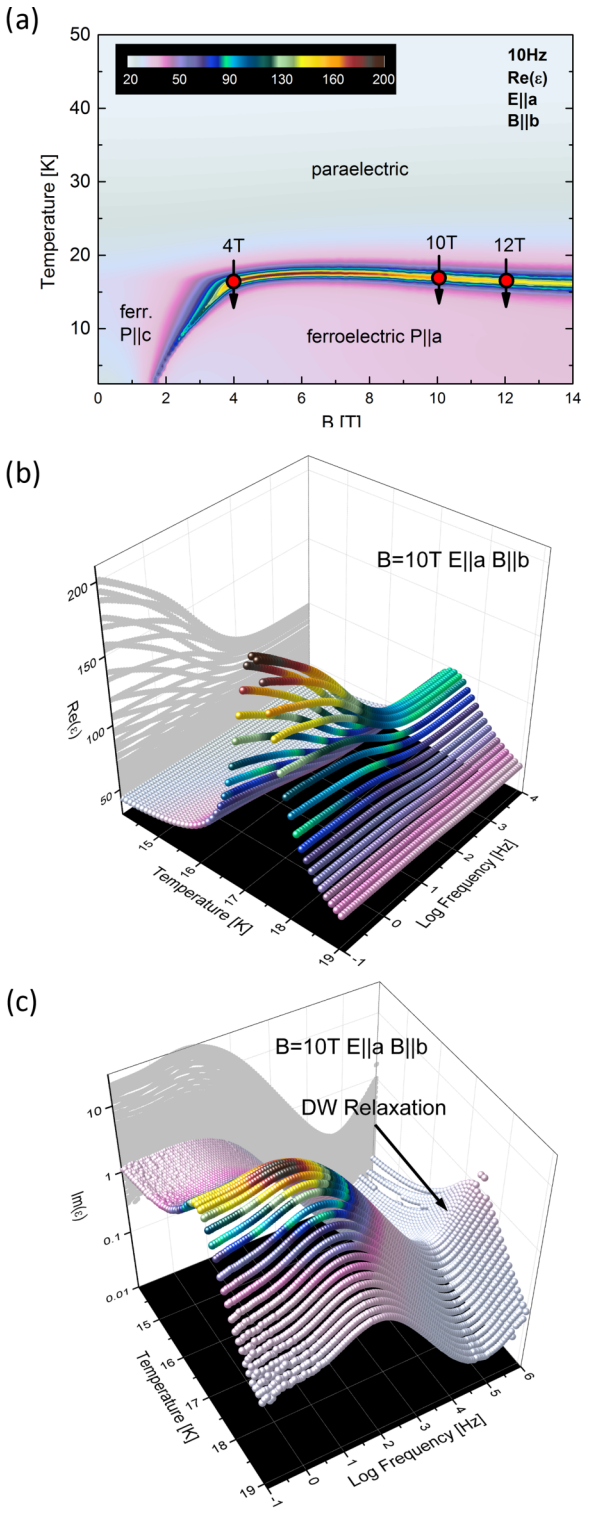

FIG. 2. (Color online) Phase diagram of magnetoelectric $DyMnO_3$ in magnetic fields along the b axis. (a) The color map is a contour plot of the real part of the dielectric constant along the a axis measured at 10 Hz. The ground state of $DyMnO_3$ in zero magnetic field is a bc cycloid with $P\|c$. In external magnetic fields, the electric polarization flops from $P\|c$ to $P\|a$. (b) Low-frequency dispersion phenomena near T_C. (c) The logarithmic plot of the imaginary part of the permittivity reveals a well-pronounced absorption in the vicinity of the paraelectric to ferroelectric phase transition and the signature of domain-wall relaxation phenomenon at higher frequencies [63].

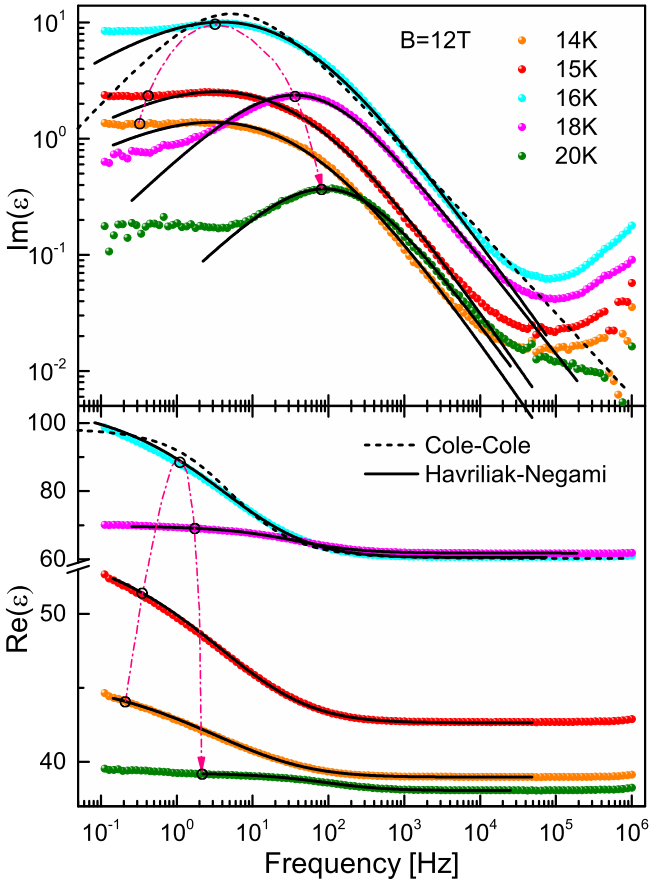

FIG. 3. (Color online) Spectrum of the dielectric permittivity in a magnetic field of $\mu_0 H = 12$ T. Typical frequency dependence of the dielectric constant, Re(ε), and dielectric loss, Im(ε), at several temperatures above ($T = 18$ and 20 K) and below ($T = 14$, 15, and 16 K) the critical temperature, $T_C \approx 17$ K (at 12 T). Black solids lines represents the fit according to the Havriliak-Negami relaxation function, Eq. (11). The dashed black line shows the fit according to the Cole-Cole equation, Eq. (12). Dash-dotted lines with open circles schematically indicate the position of the spectra with increasing temperature.

phenomenological Havriliak-Negami equation [57]:

$$\varepsilon' + \varepsilon'' = \epsilon_\infty + \frac{\Delta\varepsilon}{[1 + (i\omega\tau)^{1-\alpha}]^\beta}. \tag{11}$$

Here $\Delta\varepsilon$ is the relaxation strength, ε_∞ is the high-frequency limit of the dielectric constant, τ is the characteristic relaxation time, and α and β are the width and asymmetry parameters, respectively. A simple Debye behavior in Eq. (11) would correspond to $\alpha = 0$ and $\beta = 1$. Values of $0 < \alpha < 1$ and $0 < \beta < (1-\alpha)^{-1}$ result in broadened asymmetric loss peaks with power laws of $\omega^{1-\alpha}$ and $\omega^{-(1-\alpha)\beta}$ as the low- and high-frequency asymptotic behavior, respectively.

Since the symmetric Cole-Cole function given by

$$\varepsilon' + \varepsilon'' = \epsilon_\infty + \frac{\Delta\varepsilon}{[1 + (i\omega\tau)^{1-\alpha}]} \tag{12}$$

is intensively used as a fitting function to describe permittivity data of conventional materials as well as magnetoelectric materials [11,61], we demonstrated by the dashed line in Fig. 3

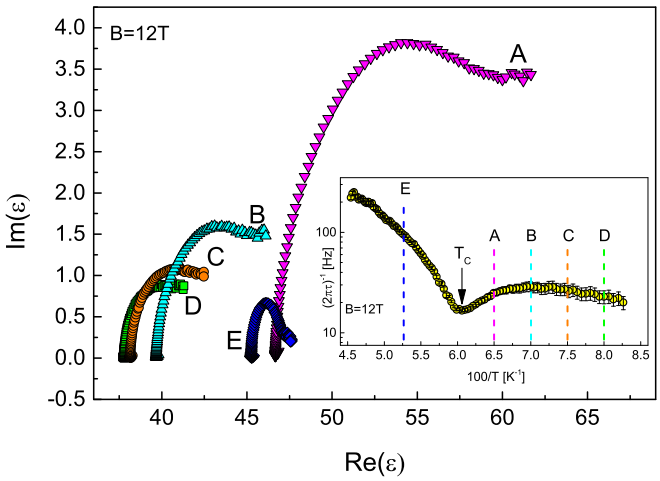

FIG. 4. (Color online) Cole-Cole plots of low-frequency relaxation. The inset shows the temperature dependence of the relaxation time in the Arrhenius representation (see Sec. IV B).

for the $T = 16$ K data that the symmetric Cole-Cole function results in a worse fit to the data compared to the Havriliak-Negami expression. Therefore, the subsequent analysis within the present work has been done according to Eq. (11). Most probably, a fitting procedure using the Cole-Cole function would lead to qualitatively similar behavior of the relaxation time and dielectric strength.

The deviations from a Debye spectral shape of the relaxation are commonly ascribed to a distribution of relaxation times. According to Eq. (8), this can be caused by fluctuations of the order parameter near the phase-transition temperature. The mean logarithmic relaxation time is related to the characteristic relaxation time by [65]

$$\langle \ln \tau_{\mathrm{HN}} \rangle = \ln \tau + \frac{\psi(\beta) + \mathrm{Eu}}{1 - \alpha}, \tag{13}$$

where $\psi(\beta)$ is the digamma function and $\mathrm{Eu} \approx 0.577$ is the Euler constant. The width of a non-Debye relaxation is defined as the variance, $\sigma^2 = \langle (\ln \tau_{\mathrm{HN}})^2 \rangle - \langle \ln \tau_{\mathrm{HN}} \rangle^2$, of the distribution of logarithmic relaxation times, and for a Havriliak-Negami function it is given by [65]

$$\sigma^2 = \frac{\psi'(\beta)}{(1-\alpha)^2} + \frac{\pi^2}{6(1-\alpha)^2} - \frac{\pi^2}{3}. \tag{14}$$

In the present work, we do not consider the relaxations by the domain walls. Compared to fluctuations on the atomic level, ferroelectric domains are typically [1] of μm size and they are responsible for the high-frequency dielectric relaxation [63,64]. Two additional arguments are in favor of the nanosized origin of the relaxation discussed here: (i) the low-frequency relaxation (Fig. 3) is well pronounced below and above T_C, and (ii) no signature of thermally activated creep motion of domain walls is evident in the Cole-Cole plots (Fig. 4). In the latter case, a linear relationship between the imaginary and real part of the permittivity with $\mathrm{Im}(\varepsilon) \propto \tan(\pi\beta/2)\,\mathrm{Re}(\varepsilon)$ and $0 < \beta < 1$ is expected [66–68].

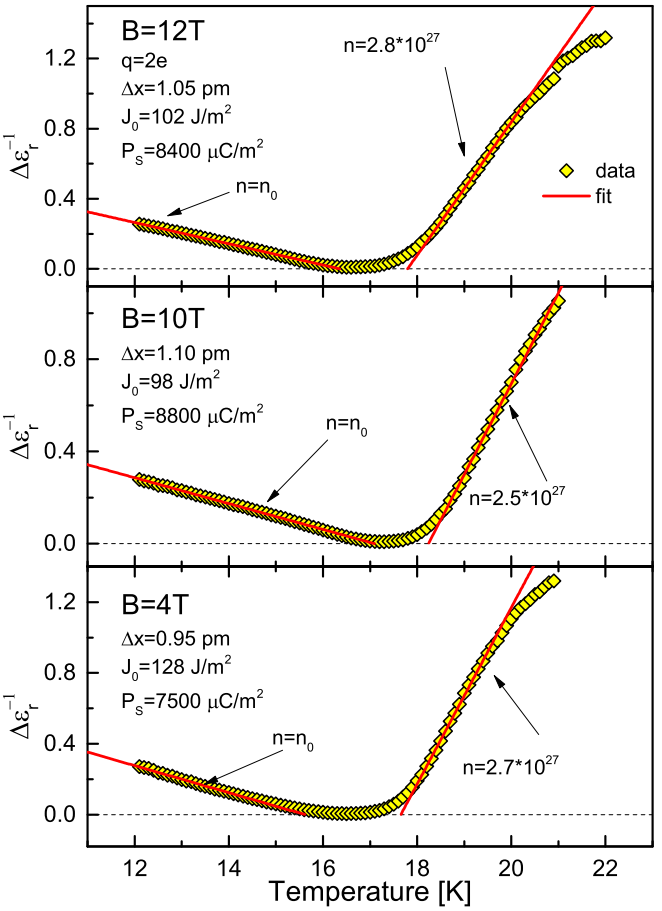

FIG. 5. (Color online) Relaxation strength in $DyMnO_3$. Inverse relaxation strength along the *a* axis of the low-frequency mode as a function of temperature for different magnetic fields along the *b* axis. The yellow symbols are obtained by the spectral analysis procedure, and the red solid line corresponds to the fit function according to Eq. (6).

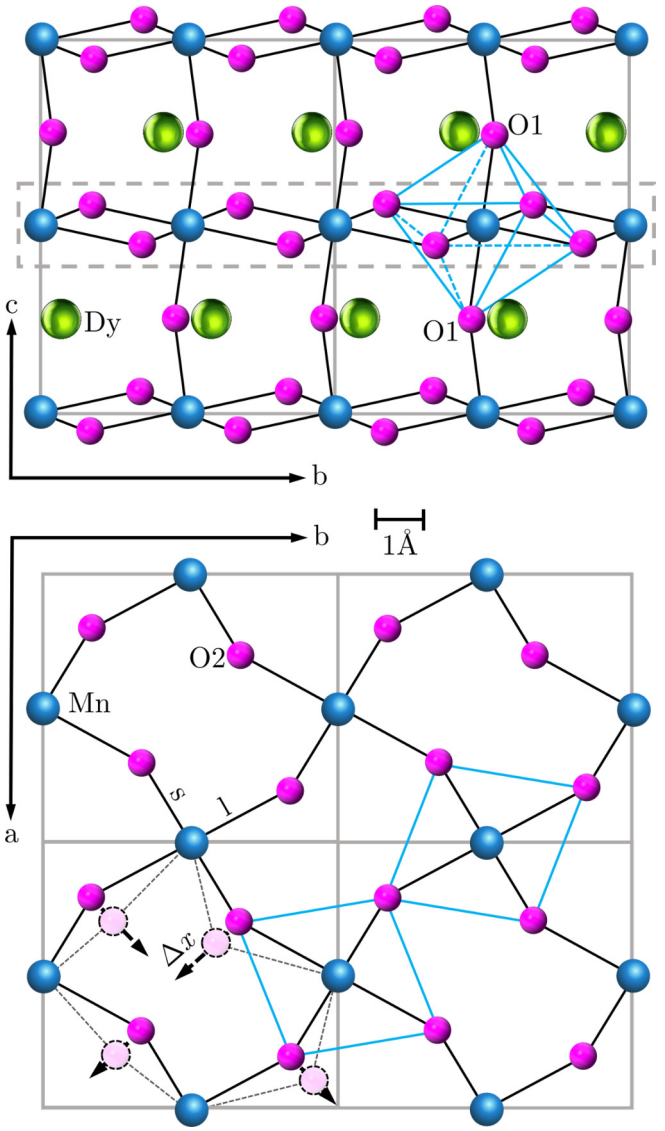

FIG. 6. (Color online) Crystal structure of the orthorhombic rare-earth manganite $DyMnO_3$. Green spheres are Dy ions, blue spheres represent Mn ions, and magenta spheres are O ions in a *Pbnm* setting. Solid gray lines mark the unit cell. Lower frame shows the *ab* plane of $DyMnO_3$ cut at the MnO_2 plane (dashed gray lines).

A. Relaxation strength

The temperature dependence of the inverse relaxation strength of the low-frequency mode is presented in Fig. 5. Dielectric permittivity diverges as the temperature approaches T_C. At the ferroelectric transition temperature, $DyMnO_3$ undergoes a phase transition accompanied by a minimum in $\Delta\varepsilon_r^{-1}$ at T_C. As predicted by Eq. (6), close to transition $\Delta\varepsilon_r^{-1}(T)$ the regions of linear dependence are shown. This behavior demonstrates critical dynamics characteristic for order-disorder phase transitions.

A significant rounding near T_C is attributed to fluctuations of the order parameter and to limitation of the correlation length close to T_C [56]. In addition, the straight lines of the model fits cross the *x* axis at temperatures deviating by about 1 K. These effects are not accounted for within the present simple model since it implies a molecular field approach and neglects fluctuations. Alternatively, a narrow temperature range near T_C may be analyzed using the formalism of critical exponents, $\Delta\varepsilon^{-1} \propto |T - T_C|^{\gamma}$. Such analysis (not shown) reveals critical exponents for the relaxation strength of the low-frequency mode near T_C between $\gamma = 1.8$ and 2.3 depending on the magnetic field. These rather high values of the critical exponents may also be seen as evidence for order-disorder type phase transitions [69].

The electric dipole moment is generated by the displacements of the O^{2-} ions, and only the ions labeled as O2 in Fig. 6 generate a static electric polarization along the *a* axis. Therefore, we assume an electric dipole density in $DyMnO_3$ equal to 2/3 of the density of O^{2-} ions in the unit cell, $n_{O^{2-}} = n_0 \sim 3.5 \times 10^{28}$ m^{-3} [70,71], and a charge of $q = 2e$, where e is the elementary charge. According to Eq. (6), the slope of $\Delta\varepsilon_r^{-1}$ is inversely proportional to $n(q\Delta x)^2 = 2P_s^2/n$ with static electric polarization along the *a* axis, $P_s = nq\Delta x/\sqrt{2}$. The factor $\sqrt{2}$ appears due to a 45° degree misalignment between the oxygen displacement and the *a* axis (Fig. 6). Hence, from the slope of $\Delta\varepsilon_r^{-1}$ at $T < T_C$

we may directly estimate the static electric polarization. The microscopic parameters of the model, Δx and J_0, are obtained from the values of the static polarization and from $J_0 = k_B T_C/2(\Delta x)^2$. These parameters are given in Fig. 5. Taking into account the simplicity of the model, the obtained values of the electric polarization agree reasonably well with directly measured data [7] $P \sim 2000\ \mu\mathrm{C/m}^2$. In addition, the obtained coupling constants coincide with the classical electric dipole energy in the Mn-O-Mn chains along the b axis, $J_0 \sim (q^2/2\pi\varepsilon_0)/(l^2+s^2)^{3/2} \sim 70\ \mathrm{J/m}^2$ (Fig. 6), with $l = 2.22$ Å and $s = 1.90$ Å being the long and short bond distances [71].

The temperature dependence of the inverse relaxation strength becomes steeper in the paraelectric phase $T > T_C$, although the model predicts the opposite behavior. This effect is evidently not captured within the assumptions of the present simple model. Two possible explanations for this behavior may be suggested in the present stage: (i) There is a change in the effective dipole density at the phase transition. In the disordered state, a large portion of the magnetic cycloid is distorted and is included in the border regions between the left- and right-rotating cycloids. The oxygen ions in these regions are effectively excluded from the relaxation process, thus reducing the effective dipole density n of the model. This explanation has been used in the fits to the data in Fig. 5, and the effective dipole density for $T > T_C$ is indicated at the fit lines. (ii) The model can be modified to account for higher-order terms [72,73]. A coupling term between the polarization and magnetization may be explicitly included in the free energy expansion, Eq. (5). The term that is always allowed by symmetry is $\gamma P^2 M^2$ where M is the magnetic order parameter. Thus the free-energy expansion near T_C, Eq. (4), can be written as

$$F = aP^2 + bP^4 - gEP + \gamma P^2 M^2, \tag{15}$$

where $a = A(T - T_C)$, and b, g, and γ are the constants of the model. In these modifications, M has to be understood as the amplitude of the transverse component of the spin cycloidal $S = (0, M\cos qy, M\sin qy)$. Applying Eq. (15) to Eq. (2) leads to

$$\frac{\partial P(t)}{\partial t} = -\Gamma(2aP + 4bP^3 - gE + \gamma P M^2). \tag{16}$$

With $E = \delta E \exp(-i\omega t)$ and $P = P_S + \delta P \exp(-i\omega t)$ and assuming that $M^2 \propto (T_C - T) = -Ca$ below T_C and $M^2 = 0$ above T_C, the relaxation strength and relaxation time become

$$\Delta\varepsilon_r^{-1} = \begin{cases} \frac{\varepsilon_0 k_B}{nq^2(\Delta x)^2}(T - T_C), & T > T_C, \\ 2(1-\gamma C)\frac{\varepsilon_0 k_B}{nq^2(\Delta x)^2}(T_C - T), & T < T_C, \end{cases} \tag{17}$$

$$(2\pi\tau)^{-1} = \begin{cases} \left[\frac{\nu_0}{\pi}\left(\frac{T-T_C}{T}\right)\exp\left(-\frac{E_A}{k_B T}\right)\right], & T > T_C, \\ 2(1-\gamma C)\left[\frac{\nu_0}{\pi}\left(\frac{T_C-T}{T}\right)\exp\left(-\frac{E_A}{k_B T}\right)\right], & T < T_C. \end{cases} \tag{18}$$

It is clear that upon adding explicitly magnetoelectric terms into the free energy, the ratio of the slopes of the relaxation strength below and above T_C deviate from the value of 2, as predicted by a simple model. In this case, the slope below T_C is governed by a new parameter $(1 - \gamma C)$ in Eqs. (17) and (18).

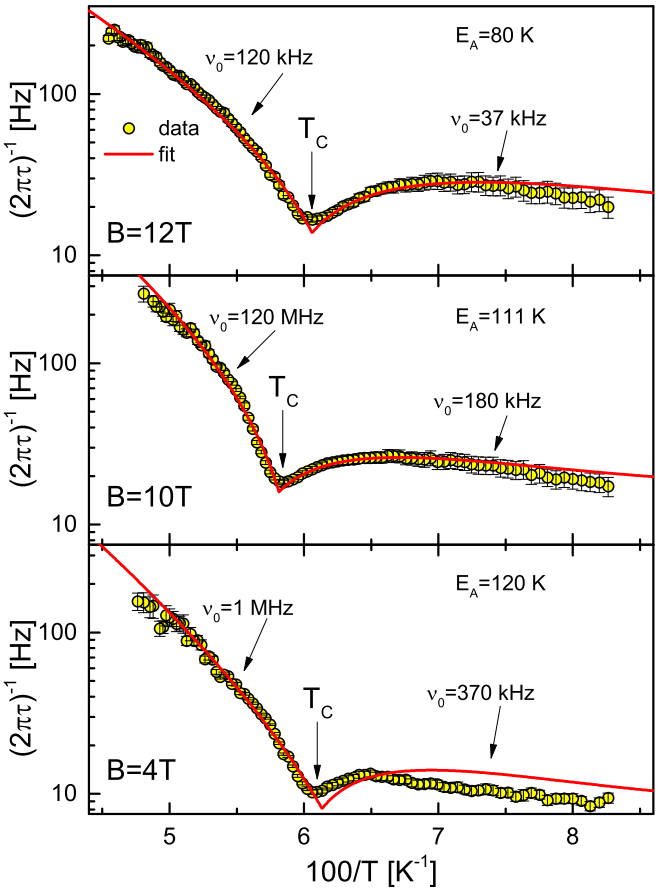

FIG. 7. (Color online) Relaxation time in $DyMnO_3$. Inverse mean relaxation time along the a axis of the low-frequency mode as a function of temperature for different magnetic fields ($B \| b$ axis). The yellow symbols are obtained by the spectral analysis procedure, and the red solid line corresponds to the fit function according to Eq. (7).

B. Relaxation time

The inverse relaxation time of the low-frequency mode obtained from the spectral analysis is shown in Fig. 7. Upon cooling from the paraelectric phase, the inverse relaxation time decreases toward T_C. Below T_C, $1/\tau$ shows a broad characteristic maximum and decreases again for low temperatures. Qualitatively, the temperature behavior of the relaxation time can be explained as a superposition of two processes: (i) temperature activated behavior with a characteristic energy of $E_a \sim 100$ K, and (ii) critical slowing down of the relaxation in the vicinity of T_C. This observation is typical for order-disorder phase transitions involving shallow double-well potentials [56,58,74].

Both processes determining the temperature evolution of the relaxation time are qualitatively well captured within the present simple model. The temperature-activated behavior, expressed by the exponential factor in Eq. (7), prevails for temperatures far from T_C and, therefore, causes an overall decrease of the relaxation time for decreasing temperature. Qualitatively similar behavior of the relaxation time was found [11] for a c-axis relaxation ($e \| c$) in $DyMnO_3$ for a transition to a bc-cycloidal magnetic ordering. The

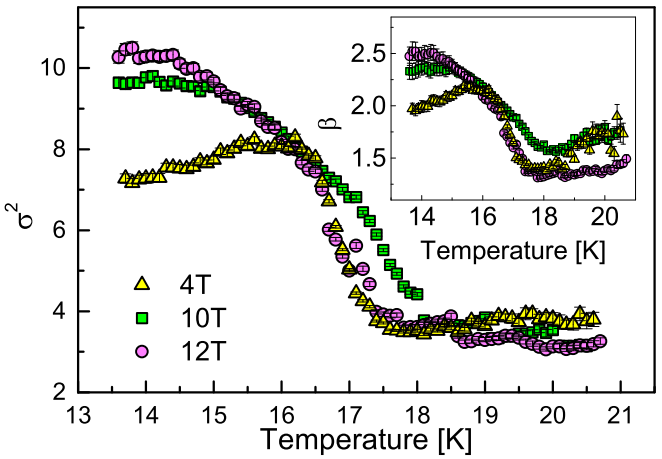

FIG. 8. (Color online) Relaxation width in $DyMnO_3$. Asymmetry and width of the low-frequency dielectric relaxation in $DyMnO_3$, obtained via Eq. (14).

$P \| c$-axis state is achieved in $DyMnO_3$ for cooling in a zero external magnetic field. It seems plausible that the c-axis relaxation in multiferroic manganites may be explained by the present model as well.

In the case of inverse relaxation time, the suggested model gives a qualitative explanation of the observed data. Equation (7) contains two temperature-dependent factors, namely the Arrhenius term $\exp[-E_A/(k_B T)]$ and the critical-slowing term $\nu_0(T - T_C)/T$. These two terms explain qualitatively the temperature dependence of the relaxation time close to the phase transition. To obtain reasonable fits to the critical behavior of the relaxation time, different values of the attempt frequency above and below T_C have been used, and a constant was added to Eq. (7). *Nota bene*, accounting for magnetodielectric effects, the slope of the inverse relaxation time is not necessarily 2; see Eq. (18). Thus the values of the attempt frequency above and below T_C can take the same value. Eventually, in addition to magnetodielectric effects, the distribution of relaxation times plays a role in explaining that feature.

The ratio of $E_A/k_B T_C \sim 5$ is further evidence of an order-disorder type phase transition [52] and is in contrast to a displacive-type phase transition where $E_A/k_B T_C \ll 1$ holds. Furthermore, $E_A/k_B \sim 100$ K corresponds well to a characteristic energy of the magnetic order as determined by a Néel temperature of $T_N \sim 39$ K [53].

Finally, Fig. 8 shows the width of the low-frequency dielectric relaxation in $DyMnO_3$, obtained via Eq. (14). The increase of the characteristic width below $T_C \sim 18$ K is clearly seen. In the ordered magnetic state, the effective length of the elementary cycloids increases, thus leading to a broader length distribution. Most probably, this also leads to the observed broadening of the dielectric relaxation.

V. DISCUSSION

The analysis of low-frequency dielectric relaxation demonstrates an overlap of two processes: critical dynamics close to T_C and activation behavior in the broader frequency range. This observation may be reasonably explained using a simple model of an order-disorder phase transition with a double-well potential. This potential reflects a dynamical switching between cycloids of opposite chirality. Several parameters of the model correlate well with the physical properties of $DyMnO_3$. Thus, the characteristic energies of magnetic ordering and the value of the static electric polarization are in agreement with known values. We note that the present experiments could be analyzed up to $T = 22$ K only. Strictly speaking, the dynamical behavior of the cycloids still may change close to T_N.

Most importantly, the present experimental data and the simple model suggest that the paraelectric sinusoidal phase in rare-earth manganate can be explained as a dynamical equilibrium of cycloids with opposite chiralities. In addition to the dielectric results, this hypothesis resolves several experimental constraints that contradicted the concept of a static sinusoidally modulated magnetic phase.

VI. CONCLUSIONS

A low-frequency relaxation mode is observed in the dielectric properties of $DyMnO_3$ multiferroic manganite, and it reveals critical behavior at the ferroelectric transition temperature, $T_C \sim 18$ K. Together with the temperature-activated relaxation rate, the observed mode may be qualitatively explained within a model for an order-disorder phase transition. The model assumes a switching between magnetic cycloids with opposite chirality, and it correlates well with the known physical properties of $DyMnO_3$.

Combining the present results with several other experiments on multiferroics, we suggest that the paramagnetic sinusoidal phase should be explained as a dynamical equilibrium between the clockwise and counterclockwise cycloidal magnetic orders. The short-range order in the paraelectric phase is transformed to a long-range cycloid at the ferroelectric transition temperature.

ACKNOWLEDGMENTS

This work was supported by the Austrian Science Funds (I815-N16, W1243).

[1] M. Fiebig, J. Phys. D **38**, R123 (2005).
[2] R. Ramesh and N. A. Spaldin, Nat. Mater. **6**, 21 (2007).
[3] Y. Tokura, Science **312**, 1481 (2006).
[4] S.-W. Cheong and M. Mostovoy, Nat. Mater. **6**, 13 (2007).
[5] N. A. Spaldin and M. Fiebig, Science **309**, 391 (2005).
[6] W. Eerenstein, N. D. Mathur, and J. F. Scott, Nature (London) **442**, 759 (2006).
[7] T. Kimura, G. Lawes, T. Goto, Y. Tokura, and A. P. Ramirez, Phys. Rev. B **71**, 224425 (2005).
[8] J. Hemberger, F. Schrettle, A. Pimenov, P. Lunkenheimer, V. Y. Ivanov, A. A. Mukhin, A. M. Balbashov, and A. Loidl, Phys. Rev. B **75**, 035118 (2007).

[9] M. Kenzelmann, A. B. Harris, S. Jonas, C. Broholm, J. Schefer, S. B. Kim, C. L. Zhang, S.-W. Cheong, O. P. Vajk, and J. W. Lynn, Phys. Rev. Lett. **95**, 087206 (2005).

[10] M. Mochizuki and N. Furukawa, Phys. Rev. B **80**, 134416 (2009).

[11] F. Schrettle, P. Lunkenheimer, J. Hemberger, V. Y. Ivanov, A. A. Mukhin, A. M. Balbashov, and A. Loidl, Phys. Rev. Lett. **102**, 207208 (2009).

[12] T. Arima, A. Tokunaga, T. Goto, H. Kimura, Y. Noda, and Y. Tokura, Phys. Rev. Lett. **96**, 097202 (2006).

[13] A. Pimenov, A. M. Shuvaev, A. A. Mukhin, and A. Loidl, J. Phys.: Condens. Matter **20**, 434209 (2008).

[14] A. Pimenov, A. Loidl, A. A. Mukhin, V. D. Travkin, V. Y. Ivanov, and A. M. Balbashov, Phys. Rev. B **77**, 014438 (2008).

[15] R. Valdes Aguilar, M. Mostovoy, A. B. Sushkov, C. L. Zhang, Y. J. Choi, S.-W. Cheong, and H. D. Drew, Phys. Rev. Lett. **102**, 047203 (2009).

[16] J. S. Lee, N. Kida, S. Miyahara, Y. Takahashi, Y. Yamasaki, R. Shimano, N. Furukawa, and Y. Tokura, Phys. Rev. B **79**, 180403 (2009).

[17] V. Cuartero, J. Blasco, J. A. Rodriguez-Velamazan, J. Garcia, G. Subias, C. Ritter, J. Stankiewicz, and L. Canadillas-Delgado, Phys. Rev. B **86**, 104413 (2012).

[18] K. Taniguchi, N. Abe, S. Ohtani, and T. Arima, Phys. Rev. Lett. **102**, 147201 (2009).

[19] H. Katsura, N. Nagaosa, and A. V. Balatsky, Phys. Rev. Lett. **95**, 057205 (2005).

[20] M. Mostovoy, Phys. Rev. Lett. **96**, 067601 (2006).

[21] I. A. Sergienko and E. Dagotto, Phys. Rev. B **73**, 094434 (2006).

[22] F. Fabrizi, H. C. Walker, L. Paolasini, F. de Bergevin, A. T. Boothroyd, D. Prabhakaran, and D. F. McMorrow, Phys. Rev. Lett. **102**, 237205 (2009).

[23] J. Voigt, J. Persson, J. W. Kim, G. Bihlmayer, and T. Brückel, Phys. Rev. B **76**, 104431 (2007).

[24] D. Mannix, D. F. McMorrow, R. A. Ewings, A. T. Boothroyd, D. Prabhakaran, Y. Joly, B. Janousova, C. Mazzoli, L. Paolasini, and S. B. Wilkins, Phys. Rev. B **76**, 184420 (2007).

[25] T. Kimura, T. Goto, H. Shintani, K. Ishizaka, T. Arima, and Y. Tokura, Nature (London) **426**, 55 (2003).

[26] T. Goto, T. Kimura, G. Lawes, A. P. Ramirez, and Y. Tokura, Phys. Rev. Lett. **92**, 257201 (2004).

[27] T. Kimura, S. Ishihara, H. Shintani, T. Arima, K. T. Takahashi, K. Ishizaka, and Y. Tokura, Phys. Rev. B **68**, 060403 (2003).

[28] O. Prokhnenko, R. Feyerherm, E. Dudzik, S. Landsgesell, N. Aliouane, L. C. Chapon, and D. N. Argyriou, Phys. Rev. Lett. **98**, 057206 (2007).

[29] O. Prokhnenko, R. Feyerherm, M. Mostovoy, N. Aliouane, E. Dudzik, A. U. B. Wolter, A. Maljuk, and D. N. Argyriou, Phys. Rev. Lett. **99**, 177206 (2007).

[30] N. Aliouane, O. Prokhnenko, R. Feyerherm, M. Mostovoy, J. Strempfer, K. Habicht, K. C. Rule, E. Dudzik, A. U. B. Wolter, A. Maljuk *et al.*, J. Phys.: Condens. Matter **20**, 434215 (2008).

[31] E. Schierle, V. Soltwisch, D. Schmitz, R. Feyerherm, A. Maljuk, F. Yokaichiya, D. N. Argyriou, and E. Weschke, Phys. Rev. Lett. **105**, 167207 (2010).

[32] S. Quezel, F. Tcheou, J. Rossat-Mignod, G. Quezel, and E. Roudaut, Physica B+C **86-88**, 916 (1977).

[33] S. B. Wilkins, T. R. Forrest, T. A. W. Beale, S. R. Bland, H. C. Walker, D. Mannix, F. Yakhou, D. Prabhakaran, A. T. Boothroyd, J. P. Hill *et al.*, Phys. Rev. Lett. **103**, 207602 (2009).

[34] A. M. Balbashov, S. G. Karabashev, Y. M. Mukovskiy, and S. A. Zverkov, J. Cryst. Growth **167**, 365 (1996).

[35] T. Mori, K. Aoki, N. Kamegashira, T. Shishido, and T. Fukuda, Mater. Lett. **42**, 387 (2000).

[36] A. M. Shuvaev, J. Hemberger, D. Niermann, F. Schrettle, A. Loidl, V. Y. Ivanov, V. D. Travkin, A. A. Mukhin, and A. Pimenov, Phys. Rev. B **82**, 174417 (2010).

[37] A. Shuvaev, V. Dziom, A. Pimenov, M. Schiebl, A. A. Mukhin, A. C. Komarek, T. Finger, M. Braden, and A. Pimenov, Phys. Rev. Lett. **111**, 227201 (2013).

[38] H. Nishimori and G. Ortiz, *Elements of Phase Transitions and Critical Phenomena* (Oxford University Press, Oxford, 2011), p. 384.

[39] M. Kardar, *Statistical Physics of Fields* (Cambridge University Press, Cambridge, 2007), p. 370.

[40] P. C. Hohenberg and B. I. Halperin, Rev. Mod. Phys. **49**, 435 (1977).

[41] U. C. Täuber, *Critical Dynamics: A Field Theory Approach to Equilibrium and Non-Equilibrium Scaling Behavior* (Cambridge University Press, Cambridge, 2014), p. 488.

[42] G. A. Smolenskii and I. E. Chupis, Sov. Phys. Usp. **25**, 475 (1982).

[43] T. Kimura, S. Kawamoto, I. Yamada, M. Azuma, M. Takano, and Y. Tokura, Phys. Rev. B **67**, 180401 (2003).

[44] G. Lawes, A. P. Ramirez, C. M. Varma, and M. A. Subramanian, Phys. Rev. Lett. **91**, 257208 (2003).

[45] G. Lawes, T. Kimura, C. M. Varma, M. A. Subramanian, N. Rogado, R. J. Cava, and A. P. Ramirez, Progr. Solid State Chem. **37**, 40 (2009).

[46] M. Kenzelmann, G. Lawes, A. B. Harris, G. Gasparovic, C. Broholm, A. P. Ramirez, G. A. Jorge, M. Jaime, S. Park, Q. Huang *et al.*, Phys. Rev. Lett. **98**, 267205 (2007).

[47] A. D. Bruce and R. A. Cowley, *Structural Phase Transitions* (Taylor and Francis, London, 1981), p. 326.

[48] A. P. Giddy, M. T. Dove, and V. Heine, J. Phys.: Condens. Matter **1**, 8327 (1989).

[49] E. K. H. Salje, Acta Crystallogr. A **47**, 453 (1991).

[50] S. Padlewski, A. Evans, C. Ayling, and V. Heine, J. Phys.: Condens. Matter **4**, 4895 (1992).

[51] S. Radescu, I. Etxebarria, and J. M. Perezmato, J. Phys.: Condens. Matter **7**, 585 (1995).

[52] M. T. Dove, Am. Miner. **82**, 213 (1997).

[53] S. Aubry, J. Chem. Phys. **62**, 3217 (1975).

[54] B. A. Strukov and A. P. Levanyuk, *Ferroelectric Phenomena in Crystals*, 1st ed. (Springer, Berlin, 1998).

[55] L. D. Landau and E. M. Lifshitz, *Statistical Physics*, 3rd ed., Pt. 1, Course of Theoretical Physics Vol. 5 (Butterworth-Heinemann, Oxford, 1975).

[56] M. E. Lines and A. M. Glass, *Principles and Applications of Ferroelectrics and Related Phenomena*, 1st ed. (Oxford University Press, Oxford, 1977).

[57] F. Kremer and A. Schönhals, *Broadband Dielectric Spectroscopy* (Springer, London, 2002), p. 729.

[58] J. A. Gonzalo, *Effective Field Approach to Phase Transitions and Some Applications to Ferroelectrics*, 2nd ed. (World Scientific, New Jersey, 2006).

[59] R. Blinc and B. Žekš, *Soft Modes in Ferroelectrics and Antiferroelectrics* (North-Holland, Amsterdam, 1974).

[60] M. Fujimoto, *The Physics of Structural Phase Transitions*, 2nd ed. (Springer, London, 2010), p. 278.

[61] D. Niermann, C. P. Grams, P. Becker, L. Bohatý, H. Schenck, and J. Hemberger, Phys. Rev. Lett. **114**, 037204 (2015).
[62] A. Pimenov, A. A. Mukhin, V. Y. Ivanov, V. D. Travkin, A. M. Balbashov, and A. Loidl, Nat. Phys. **2**, 97 (2006).
[63] F. Kagawa, Y. Onose, Y. Kaneko, and Y. Tokura, Phys. Rev. B **83**, 054413 (2011).
[64] F. Kagawa, M. Mochizuki, Y. Onose, H. Murakawa, Y. Kaneko, N. Furukawa, and Y. Tokura, Phys. Rev. Lett. **102**, 057604 (2009).
[65] R. Zorn, J. Chem. Phys. **116**, 3204 (2002).
[66] T. Braun, W. Kleemann, J. Dec, and P. A. Thomas, Phys. Rev. Lett. **94**, 117601 (2005).
[67] W. Kleemann, J. Dec, S. Miga, T. Woike, and R. Pankrath, Phys. Rev. B **65**, 220101 (2002).
[68] W. Kleemann, J. Dec, S. A. Prosandeev, T. Braun, and P. A. Thomas, Ferroelectrics **334**, 3 (2006).
[69] M. Luban, N. Wiser, and A. J. Greenfield, J. Phys. C **3**, 1 (1970).
[70] D. V. S. Muthu, A. E. Midgley, P. R. Scott, M. B. Kruger, J. R. Sahu, A. K. Sood, and C. N. R. Rao, J. Phys.: Conf. Ser. **377**, 012025 (2012).
[71] J. A. Alonso, M. J. Martnez Lope, M. T. Casais, and M. T. Fernndez Daz, Inorg. Chem. **39**, 917 (2000).
[72] A. Cano (private communication).
[73] A. Cano and A. P. Levanyuk, Phys. Rev. B **81**, 172105 (2010).
[74] D. Starešinić, K. Biljaković, P. Lunkenheimer, and A. Loidl, Solid State Commun. **137**, 241 (2006).